Adsorptive removal of phosphate from aqueous solutions using different types of red mud

Tengfei Guo, Haiquan Yang, Qingyou Liu, Hannian Gu, Ning Wang, Wenbin Yu and Yang Dai

ABSTRACT

Red mud (RM) is an industrial waste generated during production of alumina from using Bayer process or the sintering process. Four types of red mud from China were characterized for their diverse chemical and mineral compositions using ICP-AES, ICP-MS and XRD. Acid treatment was employed to obtain activated red mud, posing increased surface areas from 10–28 m^2/g to 220–350 m^2/g. RMs and ARMs were used to adsorb phosphate in solution to compare the adsorption capacity. Sample GZ3, a red mud from the sintering process presented the highest adsorption capacity among the four raw RMs, posing an adsorption capacity of 0.37 mg P/g in the solution of 1 mg P/L with a solid/solution ratio of 0.5 g: 1 L. Whereas, activated GX (AGX), a high iron Bayer red mud from diaspore bauxite, showed the highest adsorption capacity of all the ARMs, with an adsorption capacity of 1.92 mg P/g in the same condition. The dynamic studies indicate that the adsorption mainly followed the pseudo second-order model. The models of Freundlich and Langmuir were used to simulate the sorption equilibrium on GZ3 and AGX. It suggests that Freundlich model had a better correlation with GZ3 while Langmuir model fitted well with AGX.

Key words | activated red mud, adsorption capacity, dynamic model, phosphate, red mud

Tengfei Guo
Qingyou Liu
Hannian Gu (corresponding author)
Ning Wang
Yang Dai
Key Laboratory of High-temperature and High-pressure Study of the Earth's Interior, Institute of Geochemistry,
Chinese Academy of Sciences,
Guiyang 550081, China
E-mail: *guhannian@vip.gyig.ac.cn*

Tengfei Guo
Yang Dai
University of Chinese Academy of Sciences,
Beijing 100049, China

Haiquan Yang
State Key Laboratory of Environmental Geochemistry, Institute of Geochemistry,
Chinese Academy of Sciences,
Guiyang 550081, China

Wenbin Yu
State Key Laboratory of Ore Deposit Geochemistry, Institute of Geochemistry,
Chinese Academy of Sciences,
Guiyang 550081, China

Yang Dai
Red Star Development Dragon Chemical Industry Co., Ltd.,
Tongren 554001, China

INTRODUCTION

Red mud (RM) is a solid waste residue derived from the caustic digestion of bauxite ores during the production of alumina. Globally, it is estimated that less than 4 million tonnes of the 150 million tonnes of bauxite residue produced annually is used in a productive way (Evans 2016). Still, most of the red mud is disposed by landfill or pumped into holding ponds (Liu *et al.* 2014; Ye *et al.* 2015). The treatment and utilization of red mud have realistically been a significant problem in the alumina industry (Samal *et al.* 2013; Gu *et al.* 2017), for it may pose huge impacts on the environment and threats to human beings (Ruyters *et al.* 2011). Therefore, it is necessary to develop novel technologies for red mud disposal and applications.

Red mud has been demonstrated as a cheap and promising adsorbent in water treatment for removal of toxic metals, inorganic anions and organics, due to its high aluminum, iron, and calcium content, as well as its large specific surface areas and porous surface structures (Wang *et al.* 2008). Investigations of phosphate removal from aqueous solution were reported using raw red mud and activated red mud (ARM) treated with hydrochloric acid (Pradhan *et al.* 1998; Li *et al.* 2006), sulfuric acid (Mohanty *et al.* 2004), nitric acid (Huang *et al.* 2008), and treat with acidification and heat treatment (Li *et al.* 2006; Huang *et al.* 2008). It has been summarized that red mud presents varying adsorption capacity depending on the source and activation method (Wang *et al.* 2008). Generally, raw red mud exhibits

doi: 10.2166/wst.2018.182

low adsorption, and after activation (acidification and/or heat treatment), significant improvement in adsorption capacity will be achieved.

China is the largest producer of both alumina and red mud in the world, and China has approximately 30 Bayer plants of the 80 plants in the world (Liu *et al.* 2014; Evans 2016). From view of main chemical composition and alumina process, red mud in China could be classified into 4 types: sintering process red mud, lower iron diaspore red mud from Bayer process, high iron diaspore red mud from Bayer process, and gibbsite red mud (Liu *et al.* 2014). The variety of main components from different types of red mud is of imparity, for example, Al_2O_3 ranges from 2.12–33.1%, Fe_2O_3 is in the range of 6.8–71.9%, and CaO in red mud can span from 0.6–47.2% (Gräfe *et al.* 2011). In addition to this, the mineral phases of different types of red mud vary widely. Firstly, red mud consists on average of approximately 70% crystalline phases and 30% amorphous materials (Gräfe *et al.* 2011). Secondly, several categories of crystalline phases were identified including aluminosilicates, oxides and hydroxides, carbonates, sulphates etc., and each category contains numerous species with board ranges, as exemplified by aluminosilicates, which red mud contains as sodalite (4–40%), cancrinite (0–50%) and uncertain clay minerals (Evans 2016). The elemental abundance and mineralogical composition of red mud results in the distinct physical and chemical property.

As stated above, various activation or modification methods have been attempted on the application of red mud as phosphate adsorbent. However, seldom researches focus on the diversity of phosphate adsorption capacity using red mud with the various sources or different of origins. In this study, four typical kinds of red mud in China were used to reveal their diversity for phosphate adsorption capacity.

EXPERIMENT

Red mud samples and activation

Four typical red mud samples from different origins in China were collected, including GX (a high iron diaspore Bayer red mud from Guangxi, China), HN (a lower iron diaspore Bayer red mud from Henan, China), SD (a gibbsite Bayer red mud from Shandong, China) and GZ3 (a red mud from the sintering alumina process from Guizhou, China).

All samples were crushed and thoroughly homogenized for characterization and adsorption experiments. A modified method was used to activate RM proposed by Pratt & Christoverson 1982. Briefly, the four powdery RM samples were prepared with 2 M HCl (1 g:20 mL) treatments for 1 h, respectively. And then the each slurry was diluted with water and ammonia was added slowly to neutralize until a stable pH of 7.5 was obtained. After cooling, centrifuging, and washing, the precipitates was obtained. Correspondingly, the dried activated RMs were referred to as AGX, AHN, ASD and AGZ3.

Analysis and characterization

The chemical compositions of the RM and ARM samples were determined by Inductively Coupled Plasma – Atomic Emission Spectroscopy (ICP-AES, Agilent VISTA) and Inductively Coupled Plasma – Mass Spectrometry (ICP-MS, Agilent 7,700×). A prepared sample (weigh up to 0.2500 g) was added with a few drops of water in a teflon container, subsequently, was digested with a series of concentrated acids,10 mL perchloric, 10 mL nitric and 2 mL hydrofluoric acids on the condition of heating. The residue was leached with dilute hydrochloric acid and diluted to volume, which was then analyzed by ICP-AES (data shown in Table 1 as %) and ICP-MS (data shown in Table 1 as μg/g).

All of the RMs and ARMs were characterized by powder X-ray diffraction (XRD) and Brunaeur Emmett and Teller (BET) analysis. Powder XRD measurements were performed using a PANalytical Empyrean diffractometer with Cu Kα radiation. Samples were prepared by compaction into a silicon sample holder and a 2θ range between 5° and 70° was scanned. BET surface areas and total pore volume (listed in Table 2) were determined by nitrogen adsorption-desorption at the liquid nitrogen temperature using an automatic specific surface area and aperture analyzer (Quantachrome, Autosorb-iQ2). All samples were degassed at 150 °C for 10 h before analysis. The BET equation was applied to calculate the surface areas.

Adsorption experiments

The phosphate solution was prepared as a stock solution for adsorption experiments with potassium dihydrogen phosphate (Guaranteed Reagent, Tianjin Kemiou Chemical Reagent Co., Ltd., China). The dynamic experiments were conducted in 1,000 ml stoppered conical flasks containing 1 mg/L phosphate solution with 0.5 g original RM or ARM inside. The flasks were placed in a Water-bathing Constant Temperature Vibrator for a particular period of time and shaken gently. Liquid samples were collected at various

Table 1 | Chemical composition of four RM and ARMs

Element and unit	Al %	Ca %	Fe %	Na %	Ti %	K %	Mg %	S %	P μg/g	Ba μg/g	Mn μg/g	Sr μg/g
GX	7.59	9.66	20.1	3.75	3.89	0.18	0.34	0.23	700	80.0	983	149.5
HN	10.40	12.0	6.45	4.96	2.34	1.68	0.76	0.52	930	150	206	725
SD	8.79	0.97	21.5	6.97	2.47	0.14	0.04	0.12	530	50.0	423	27.9
GZ3	5.15	21.5	5.34	2.42	2.19	1.11	0.55	0.82	1,100	250	160	1,600
AGX	6.97	2.08	19.95	0.30	3.86	0.06	0.08	0.10	640	60.0	883	48.6
AHN	10.30	2.23	6.92	0.49	2.43	1.19	0.21	0.15	910	120	212	191
ASD	9.49	0.40	19.30	0.43	2.16	0.09	0.04	0.05	500	40	364	14.2
AGZ3	7.50	3.13	8.12	0.16	3.69	0.15	0.09	0.12	1,630	170	182	300

Table 2 | pH and surface area of various red mud samples

Samples	pH initial	pH final	BET (m^2/g)	Total pore volume (cm^3/g)
GX	10.0	8.3	10.312	0.0732
HN	11.9	8.8	10.050	0.0874
SD	10.7	9.4	27.955	0.1222
GZ3	12.5	10.2	26.130	0.1809
AGX	8.0–8.5	7.7	232.634	0.1882
AHN	8.0–8.5	7.7	219.607	0.2406
ASD	8.0–8.5	7.7	258.002	0.2027
AGZ3	8.0–8.5	8.2	350.818	0.3198

time intervals and the concentrations of phosphate were determined by a Jasco V-550 UV/vis spectrophotometer at λ of 700 nm. A standard curve was obtained by measuring the absorbance of phosphate concentration ranging from 0.01–1.20 mg P/L as the basis to calculate the concentration of samples.

The isothermal adsorption tests were performed by adding 0.125 g of samples in a 250 mL of 0.5–10 mg P/L of KH_2PO_4 solution for 6 h at the same temperature. The equilibrium time was determined according to preliminary experiments. The concentration of phosphate was measured using the spectrophotometry described above. All experiments were in duplicate so as to obtain more accurate results.

RESULTS AND DISCUSSION

Chemical and mineral composition

The chemical composition of the four RMs used in this study and ARMs is shown in Table 1. This method cannot provide the results of silicon in target samples. However, the content of silicon for RM samples has a narrow range of ca. 6–9% as previous reported (Gu *et al.* 2016). Table 1 shows that GX (a high iron diaspore Bayer red mud) and SD (a Bayer red mud generated from gibbsite) contain higher iron than HN (a low iron diaspore Bayer red mud) and GZ3 (a red mud from sintering process and low iron). Another variety of the content is calcium, which is commonly added to replace sodium for saving on costs in the process. SD (the gibbsite Bayer red mud) has a calcium content of only 0.97%, and GZ3 contains as high as 21.5% of calcium, indicative that massive lime was added in the sintering alumina process. With regard to the composition of ARMs, calcium and sodium were removed heavily after the acid treatment. Iron and aluminium were still the dominant composition in treated samples; meanwhile, titanium almost remained the ARMs. In addition, it is judged that silicon contents increased compared to original samples.

RM and ARM samples were characterized by powder XRD (seen in Figure 1). The XRD pattern of GX and SD has been reported for iron-containing phase identity (Gu *et al.* 2016). Given the fact that RM samples are complex mixtures containing a number of different components, identification and quantity of the exact composition of the samples by XRD can be highly challenging and not fully reliable (Gräfe *et al.* 2011; Gu *et al.* 2016). As previous reported, the main peaks on the pattern of GX, HN and SD were matched well with hematite, whilst GZ3 and HN consisted of compounds of calcium and/or sodium aluminates or silicates, such as cancrinite and nepheline. Generally, the mineral phase compositions of the low iron red mud were more complex and more difficult to confine than those of high iron red mud. Basically, the mineral phases of ARM samples were quite different from the raw RMs. It can be seen that hematite in SD and calcite in

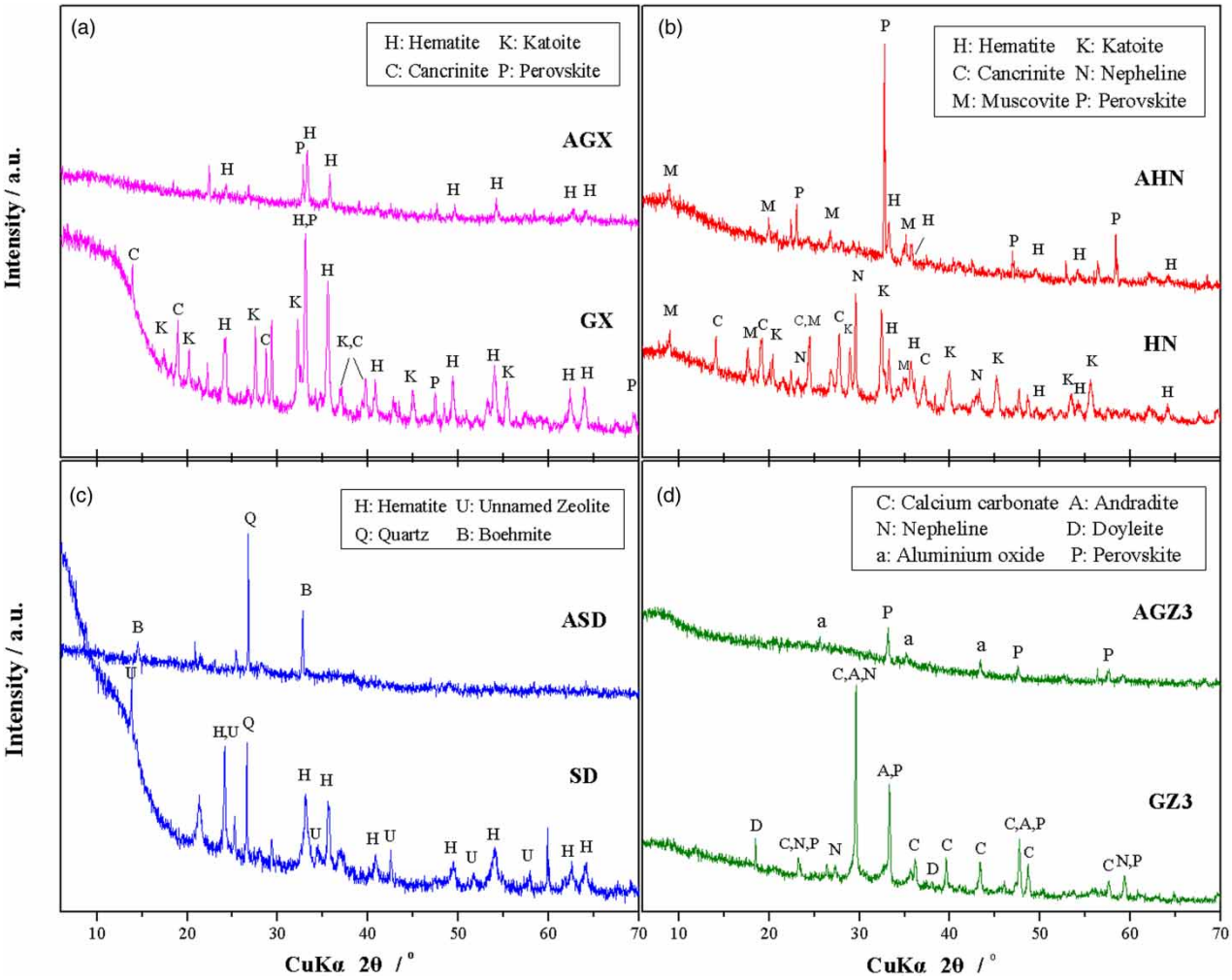

Figure 1 | XRD patterns of RMs and ARMs.

GZ3 were removed or changed after the treatment of acid activation.

Dynamic adsorption and equilibrium

The results of dynamic adsorption of phosphate on 4 raw RM samples are presented in Figure 2. HN, SD and GZ3 reached their adsorption equilibrium in last 2 or 3 hours, while the equilibrium of GX was obtained 2 h earlier. The equilibrium time depends on the decline of the diffusion rate. Another point of difference between GX and the other three RMs was the phosphate adsorbed quantity (Q) at the first 10 min. This can be explained by the difference of solution pH. Previous research has demonstrated that increasing the pH resulted in a decrease phosphate adsorption (Pradhan *et al.* 1998). From Table 2, pH value (10.0) of GX was lower than the other three and it could promote the phosphate adsorption at the beginning stage. However, from the view of different RM samples in this

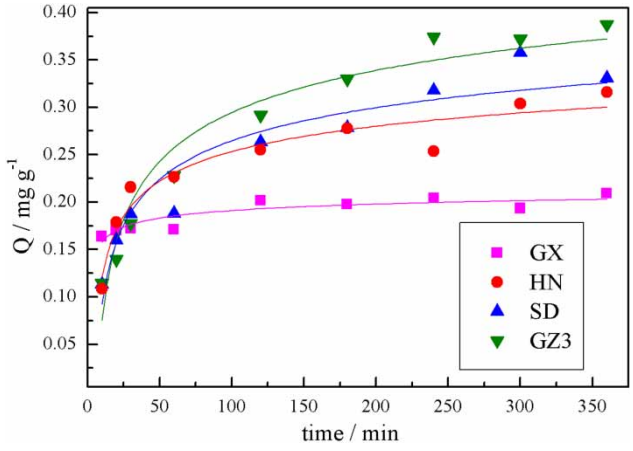

Figure 2 | Dynamic adsorption of phosphate on RM.

study, pH is not the only factor that influences the adsorption capacity. As seen from the Figure 2, GZ3 achieved the greatest adsorption capacity among all the four types of RM samples though it had the highest pH. The adsorption capacity of GZ3 at 6 h was ca. 0.37 mg P/g, much higher than GX with a value of 0.21 mg P/g. Notably, GZ3 was the only RM that obtained from the sintering alumina process, and also calcium carbonate presented in GZ3 as the dominant phase rather than hematite. It is reported that calcite can remove phosphate in both acidic and strong basic solutions (Liu *et al.* 2012). Therefore, given a range of pH value, the adsorption capacity of various raw red mud samples mainly depends on the type of red mud, which possess surface characteristics (surface areas and pore volumes) and various chemical and mineral compositions.

Figure 3 presents the results of dynamic adsorption of phosphate on four ARMs. In comparison to Figure 2, it can be observed that all ARM samples reached equivalence zone in the adsorption dynamic curve earlier than their raw RMs. Meanwhile, adsorption capacity of all ARM samples remarkable improved. The adsorption capacity of AGX at 6 h was ca. 1.92 mg P/g and 9 times more than of GX, while AGZ3 had an adsorbed amount of 1.50 mg P/g, 4 times of GZ3. The adsorption capacities of RM were close to previous literature (Huang *et al.* 2008), while ARMs in this study performed higher adsorption capacities than those activated with different methods reported by Huang *et al.* (2008). This could be assigned to the increased pore volumes. In comparison to previous literature, ARM in this study had bigger increments of BET surface areas and total pore volumes. With regard to the performance of RM and ARM, on the one hand the activation method reduced the negative charges by neutralizing the alkaline properties of RM surface and resulted in enhancements the adsorption of phosphate (Wang *et al.* 2005; Huang *et al.* 2008), on the other hand the surface areas (BET data seen in Table 2) of ARM notably increased after the treatment of activation process, which would give a positive influence on adsorption capacity. These changes might be the main reasons that the enhancement of adsorption capacity emerged between RMs and ARMs.

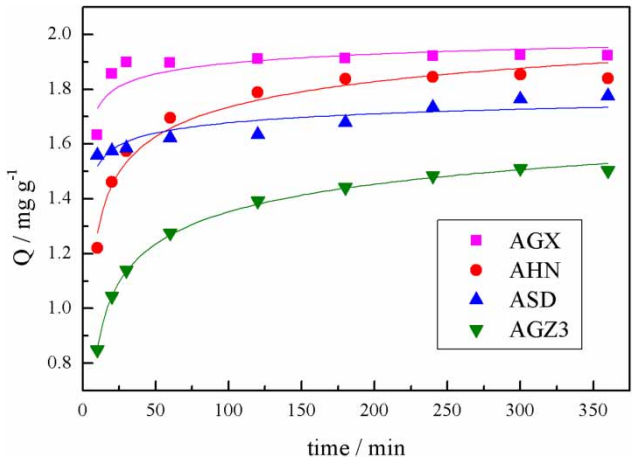

Figure 3 | Dynamic adsorption of phosphate on ARMs.

As mentioned, calcite can remove phosphate (Liu *et al.* 2012). XRD patterns shows that after acid treatment, carbonate in AGZ3 disappeared, and AGZ3 lost the contribution for phosphate removal from carbonate. Due to this reason, in comparison to other ARM adsorbents, AGZ3 performed less increment although it had high BET surface and total pore volume (Table 2). Based on the same treatment, adsorption capacity of ASD and AHN performed slightly lower than that of AGX. However, we should return to the types of samples to understand the difference of adsorption capacity. Overall, the adsorption mechanism of red mud is complex, and the dominant factor in the adsorption process is not clear. Chemical and mineral compositions reflect the surface structures that red mud samples included and worked in the adsorption process. Surface structures of RM and ARM samples depend on the types of red mud. The synergy can explain the difference of adsorption capacities that ARM adsorbents performed.

Based on those tests, the experimental results were employed to derive the dynamic parameters using models of the pseudo first-order and pseudo second-order mechanism (seen in Table 3). It is seen that the pseudo first-order model did not show a good agreement with the experimental data ($q_{e,exp}$), whereas the second-order model provided a close fit, with a regression coefficient R^2 of greater than 0.99 in most cases. In this study, the pseudo second-order mode was considered as a better-fit model for phosphate adsorption rather than pseudo first-order. In adsorption processes, a pseudo second-order mode is generally interpreted to mean that the mechanism of the process is mainly controlled by chemical bonding or chemisorption (Bhakat *et al.* 2006; Huang *et al.* 2008). Figure 4 shows the curves of linear fitting for pseudo second-order dynamics of phosphate adsorption. As before literatures reported (Bhakat *et al.* 2006; Huang *et al.* 2008), the cause of phosphate adsorption onto the RMs and ARMs involves valency forces through sharing or exchange of electrons between sorbate and sorbent.

Table 3 | Dynamic parameters for P adsorption on RM and ARM

		Pseudo first-order			Pseudo second-order		
Samples	$q_{e,exp}$	k_1	$q_{e,cal}$	R^2	k_2	$q_{e,cal}$	R^2
GX	0.2093	0.0091	0.0479	0.8512	0.8196	0.2072	0.9980
HN	0.3039	0.0061	0.1296	0.6691	0.3380	0.2753	0.9940
SD	0.3576	0.0071	0.2392	0.9682	0.1010	0.3391	0.9830
GZ3	0.3721	0.0119	0.3282	0.9520	0.0589	0.4176	0.9870
AGX	1.9243	0.0146	0.0988	0.7839	0.4891	1.9279	1.0000
AHN	1.8534	0.0183	0.5583	0.9810	0.0867	1.8914	0.9999
ASD	1.7634	0.0073	0.2325	0.8965	0.1889	1.7292	0.9991
AGZ3	1.5107	0.0129	0.6037	0.9848	0.0638	1.5330	0.9996

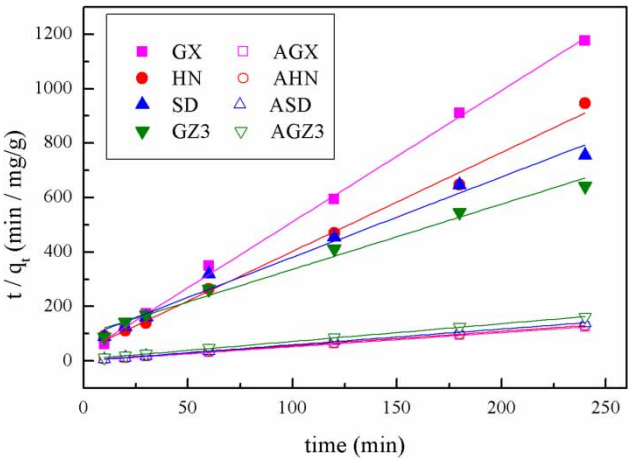

Figure 4 | Pseudo second-order dynamics of phosphate adsorption on RMs and ARMs.

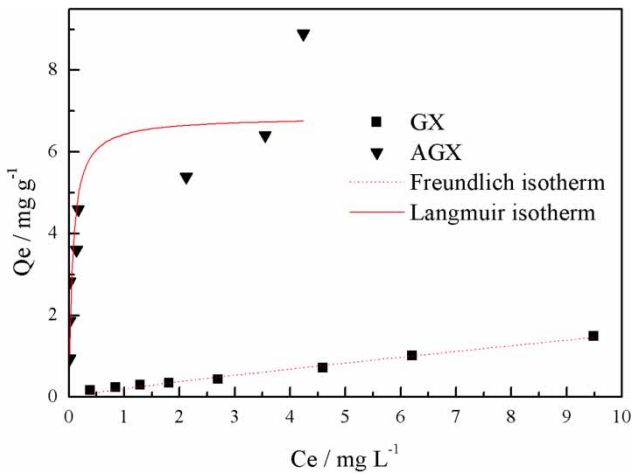

Figure 5 | Adsorption isotherm of GX and AGX.

Adsorption isotherm

Since GZ3 and AGX had a highest $q_{e,exp}$ in the solution of 1 mg P/L, the equilibrium adsorption isotherm for phosphate on these two groups (GZ3 and AGZ3, GX and AGX) was investigated in this study. The results of adsorption isotherm are shown in Figures 5 and 6. Meanwhile, models of Langmuir and Freundlich isotherms were applied to describe the equilibrium adsorption of adsorbates from liquid solution. The isotherm parameters of adsorption using the Langmuir and Freundlich isotherms are shown in Table 4.

Comparison between experimental data and isotherm models shows that the Freundlich isotherm is more suitable for the experimental data of GX, GZ3 and AGZ3, whilst Langmuir isotherm was in agreement with AGX well. Both Freundlich and Langmuir model were suggested to

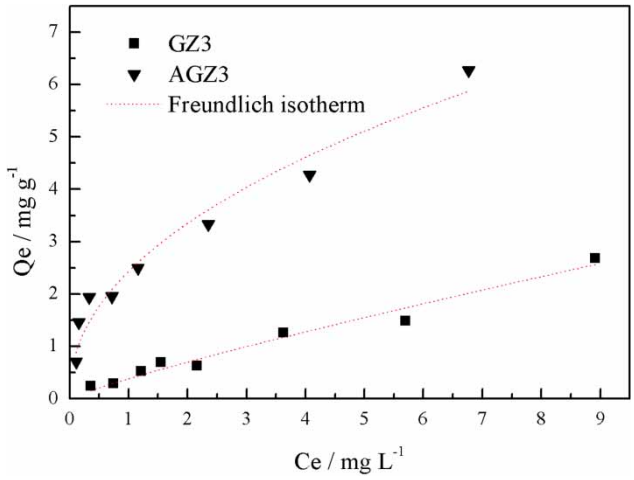

Figure 6 | Adsorption isotherm of GZ3 and AGZ3.

Table 4 | Adsorption isotherm parameters for GX(AGX) and GZ3(AGZ3)

Sample	Model	Parameters		R^2
GX	Langmuir	k = 0.0904	Qm = 2.8490	0.4680
	Freundlich	K = 0.2622	1/n = 0.6966	0.9595
AGX	Langmuir	k = 5.7500	Qm = 7.6278	0.9286
	Freundlich	K = 5.4075	1/n = 0.2608	0.7924
GZ3	Langmuir	k = 0.0827	Qm = 5.4765	0.4109
	Freundlich	K = 0.4423	1/n = 0.7551	0.9556
AGZ3	Langmuir	k = 0.7284	Qm = 6.6578	0.8852
	Freundlich	K = 2.4831	1/n = 0.4307	0.9083

follow the phosphate adsorption process based on red mud samples (Pradhan *et al.* 1998), and in some case Freundlich model fitted well (Huang *et al.* 2008). Since Freundlich model is an empirical equation employed to describe heterogeneous systems (Li *et al.* 2006), it would be concluded that mixtures compositions of GX, GZ3 and AGZ3 played a role in the phosphate adsorption. Langmuir isotherm model assumes uniform energies of sorption onto the surface with no transmigration of adsorbate in the plane of the surface (Li *et al.* 2006). In this study, hematite was considered as the dominant material in AGX that worked for phosphate adsorption.

CONCLUSION

Four types of red mud from China were characterized, and their chemical compositions and mineral phases were diverse. Acid activation changed the main mineral compositions of RM as well as increased the BET surface area and total pore volume. RM and ARM can be used as adsorbent materials on phosphate, but they exhibited different adsorption capacities. Among the raw RM samples, GZ3, red mud from sintering process, presented a highest adsorption capacity of 0.37 mg P/L in 1 mg P/L solution at a nature pH at room temperature. After activation, AGX (activated from a high iron diaspore Bayer red mud) showed a greatest adsorption capacity of 1.92 mg P/L in the same conditions.

The adsorption dynamics were described by the pseudo second-order model, indicative that the mechanism of the process was mainly controlled by chemical bonding or chemisorption. The Freundlich isotherm provided a better fitting for GZ3, suggesting multiphase compositions play a role in the phosphate adsorption process. Langmuir isotherm was in agreement with AGX well, and hematite was suggested as the main material functioning.

ACKNOWLEDGEMENTS

The work was financially supported by National Natural Science Foundation of China (Grant No. 41402039), Guizhou Provincial Science and Technology Foundation (No. [2016]1155) and Guizhou Science and Technology Major Program (No. [2016]3015). The authors are grateful to Dr Y. Meng for the XRD analytical test. H. Gu acknowledges Dr W. Liu who provided the samples of GX, HN and SD.

REFERENCES

Bhakat, P. B., Gupta, A. K., Ayoob, S. & Kundu, S. 2006 Investigations on arsenic(V) removal by modified calcined bauxite. *Colloids and Surfaces A: Physicochemical and Engineering Aspects* **281**, 237–245.

Evans, K. 2016 The history, challenges, and new developments in the management and use of bauxite residue. *Journal of Sustainable Metallurgy* **2** (4), 316–331.

Gräfe, M., Power, G. & Klauber, C. 2011 Bauxite residue issues: III. Alkalinity and associated chemistry. *Hydrometallurgy* **108**, 60–79.

Gu, H., Hargreaves, J. S. J., McFarlane, A. R. & MacKinnon, G. 2016 The carbon deposits formed by reaction of a series of red mud samples with methanol. *RSC Advances* **6** (52), 46421–46426.

Gu, H., Wang, N., Yang, Y., Zhao, C. & Cui, S. 2017 Features of distribution of uranium and thorium in red mud. *Physicochemical Problems of Mineral Processing* **53** (1), 110–120.

Huang, W., Wang, S., Zhu, Z., Li, L., Yao, X., Rudolph, V. & Haghseresht, F. 2008 Phosphate removal from wastewater using red mud. *Journal of Hazardous Materials* **158**, 35–42.

Li, Y., Liu, C., Luan, Z., Peng, X., Zhu, C., Chen, Z., Zhang, Z., Fan, J. & Jia, Z. 2006 Phosphate removal from aqueous solutions using raw and activated red mud and fly ash. *Journal of Hazardous Materials* **137**, 374–383.

Liu, Y., Sheng, X., Dong, Y. & Ma, Y. 2012 Removal of high-concentration phosphate by calcite: effect of sulfate and pH. *Desalination* **289**, 66–71.

Liu, W., Chen, X., Li, W., Yu, Y. & Yan, K. 2014 Environmental assessment, management and utilization of red mud in China. *Journal of Cleaner Production* **84**, 606–610.

Mohanty, S., Pradhan, J., Das, S. N. & Thakur, R. S. 2004 Removal of phosphorus from aqueous solution using alumized red mud. *International Journal Environmental Studies* **61**, 687–697.

Pradhan, J., Das, J., Das, S. & Thakur, R. S. 1998 Adsorption of phosphate from aqueous solution using activated red mud. *Journal of Colloid and Interface Science* **204**, 169–172.

Pratt, K. C. & Christoverson, V. 1982 Hydrogenation of a model hydrogen-donor system using activated red mud catalyst. *Fuel* **61**, 460–462.

Ruyters, S., Mertens, J., Vassilieva, E., Dehandschutter, B., Poffijn, A. & Smolders, E. 2011 The red mud accident in Ajka (Hungary): plant toxicity and trace metal bioavailability in red mud contaminated soil. *Environmental Science & Technology* **45**, 1616–1622.

Samal, S., Ray, A. K. & Bandopadhay, A. 2013 Proposal for resources, utilization and processes of red mud in India-a review. *International Journal of Mineral Processing* **118**, 43–55.

Wang, S., Boyjoo, Y., Choueib, A. & Zhu, Z. 2005 Removal of dyes from aqueous solution using fly ash and red mud. *Water Research* **39**, 129–138.

Ye, J., Cong, X., Zhang, P., Hoffmann, E., Zeng, G., Wu, Y., Zhang, H. & Fang, W. 2015 Preparation of a new granular acid-activated neutralized red mud and evaluation of its performance for phosphate adsorption. *ACS Sustainable Chemistry & Engineering* **3** (12), 3324–3331.

First received 18 October 2017; accepted in revised form 10 April 2018. Available online 20 April 2018